EPJ Quantum Technology
a SpringerOpen Journal

COMMENT   **Open Access**

Modelling carbon capture on metal-organic frameworks with quantum computing

Gabriel Greene-Diniz[1], David Zsolt Manrique[1], Wassil Sennane[2], Yann Magnin[3], Elvira Shishenina[4,2], Philippe Cordier[2], Philip Llewellyn[3], Michal Krompiec[1], Marko J. Rančić[2*] and David Muñoz Ramo[1]

*Correspondence:
marko.rancic@totalenergies.com
[2]TotalEnergies, OneTech, One R&D,
8 Boulevard Thomas Gobert, 91120
Palaiseau, France
Full list of author information is
available at the end of the article

Abstract

Despite the recent progress in quantum computational algorithms for chemistry, there is a dearth of quantum computational simulations focused on material science applications, especially for the energy sector, where next generation sorbing materials are urgently needed to battle climate change. To drive their development, quantum computing is applied to the problem of CO_2 adsorption in Al-fumarate Metal-Organic Frameworks. Fragmentation strategies based on Density Matrix Embedding Theory are applied, using a variational quantum algorithm as a fragment solver, along with active space selection to minimise qubit number. By investigating different fragmentation strategies and solvers, we propose a methodology to apply quantum computing to Al-fumarate interacting with a CO_2 molecule, demonstrating the feasibility of treating a complex porous system as a concrete application of quantum computing. We also present emulated hardware calculations and report the impact of device noise on calculations of chemical dissociation, and how the choice of error mitigation scheme can impact this type of calculation in different ways. Our work paves the way for the use of quantum computing techniques in the quest of sorbents optimisation for more efficient carbon capture and conversion applications.

Keywords: Quantum computing; NISQ; Carbon capture; Climate change; Quantum algorithms

1 Introduction

The capture of carbon dioxide at various concentrations, from industrial sources or from the air, can be performed using nanoporous adsorbent materials. However, the question of accurately identifying specific CO_2 sorption mechanisms in solids is an important step for materials design optimisation. Up to now, the use of first principles or *ab initio* calculations to accurately describe molecular interactions in such systems often yields imprecise solutions [1, 2]. Due to the natural way in which many-body interactions can be treated, as well as the sheer size of the computational space, quantum computing represents a future alternative in modelling such systems. Whilst contemporary quantum computing solvers are successful in capturing many-body interactions of a chemical system, the number of orbitals is limited such that usually only small molecules can be treated. In this work, we develop a strategy for accurately describing molecular interactions with quantum comput-

ers with a special emphasis on modelling CO_2 capture with Metal-Organic Frameworks (MOFs), a candidate for scalable carbon-capture technology. We anticipate that the insights obtained with our study can be used to feed empirical force field calculations. Here, the aluminium fumarate MOF is decomposed into interacting fragments, and the fragment containing the adsorbing Al site is treated with quantum computing. The interaction of CO_2 with the aluminium active site is modelled using the Variational Quantum Eigensolver (VQE) - a hybrid quantum classical algorithm. These results are compared to classical methods and highlight which quantum solver and fragmentations can be successful in capturing many-body interactions in MOF-CO_2 systems. The results obtained allow us to get an insight into the complex mechanism of guest-host bond formation.

Global warming can be considered as the greatest challenge of our century. A global energy transition based on low-carbon emissions is thus urgently needed to limit global warming below 2°C in the next few decades. To tackle deleterious greenhouse gas effects and particularly CO_2 contributing to ∼70% of the overall emissions [3], drastic changes have to be made. This includes the swift introduction of policies and fundamental political changes in order to rapidly shift from the use of fossil fuels to low-carbon energy sources.

Along with avoiding fossil carbon and reducing its use, for example with renewable energy, carbon capture and storage (CCS) is considered a complementary strategy to curb greenhouse gas emissions, as a robust means to target the decarbonation challenge [4, 5]. In CCS, the first step is to capture the CO_2 either from anthropogenic point sources, from bioenergy conversion or from atmosphere by direct air capture to remove current and historical emissions [6, 7]. CO_2 adsorption in solid porous sorbents such as carbon [8], zeolites [9], covalent-organic polymers [10], covalent-organic frameworks [11] and metal-organic frameworks (MOFs) [12] has drawn widespread attention due to their low energy requirements [13]. MOFs are nano- and/or mesoporous synthetic crystals, composed of metal ion/oxide nodes coordinated by organic ligands. They can be compared to molecular LEGO, offering a quasi-infinite tunability with respect to their pore sizes and reactivity depending on their metal, ligand type and overall chemistry [14]. MOFs have emerged as promising candidates for the carbon capture technology of the near future [15], due to a unique versatility, enhanced by emerging machine learning approaches to rapidly propose structures [16].
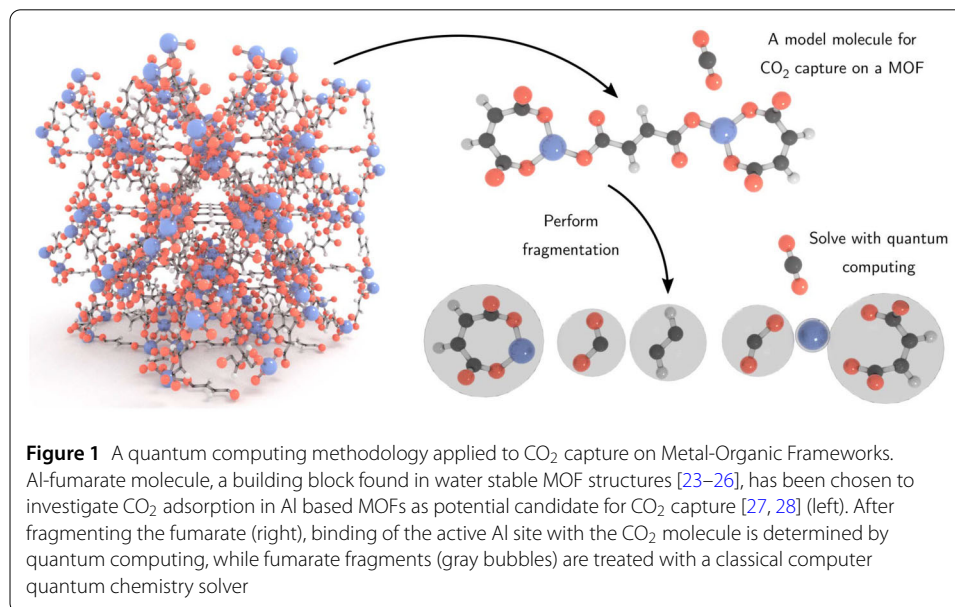
Nevertheless, water, often present in industrial flue gases or in the air, can strongly affect CO_2 capacity and selectivity. To predict properties of next generation MOFs, high throughput techniques are usually employed, which consist of screening of a very large number of hypothetical MOF structures, followed by the determination of isotherms to find the best candidate for targeting applications [17]. In the latter, thermodynamic calculations are based on empirical force fields [18, 19], adjusted from density functional theory (DFT) or *ab initio* techniques, and then used in Monte Carlo algorithms. DFT has been successful in predicting a number of material properties, however, its application is based on approximate functionals, known to not fully capture electronic structure when van der Waals interactions are present [2], such as in the case of CO_2 capture on MOFs [1, 20, 21]. In particular, MOF point charges participating in adsorbate-adsorbent interactions have been shown to strongly depend on the choice of DFT functional, basis set size, *etc* [21, 22]. *Ab initio* algorithms, that can in some cases reach an exact solution of the Schrödinger equation, are time consuming and remain limited for many-body systems, where solutions in practice do not fully converge. Upscaling simulations based on such

techniques yield in some cases spurious isotherm predictions, especially when accounting for ubiquitous moisture [22, 29, 30], that cannot be neglected in a screening process because of its critical role in applications [31].

Quantum computing is a promising tool for many-body systems, chemistry, materials sciences, *etc* [32–38]. Such advanced techniques, benefiting from lower levels of approximations could thus improve the quest in MOF design, with the high degree of accuracy required when such sorbents interact with rich adsorbates media. In quantum computers, qubit (quantum version of the classical bit) states can take an infinity of values between 0 and 1 due to superposition phenomena. In quantum simulations, qubit states are manipulated using quantum gates to mimic electronic wavefunctions, while entanglement phenomena allow for high computing efficiency. Such an approach is in principle ideal for working with electrons, since the exponentially large space of electronic states can be captured by the exponentially large Hilbert space of qubit states. This is a key advantage over classical simulations which are hindered by the exponential scaling of the electronic structure problem. However, current noisy intermediate scale quantum computing hardware (NISQ) is limited by the loss of quantum properties (quantum decoherence), due to undesired interactions of qubits with their environment, restricting first principles simulations to small and simple systems [39].

2 Results and discussions

To overcome the limitations of current day quantum computing methods, a fragmentation technique based on Density Matrix Embedding Theory (DMET) [40, 41] has been proposed as a robust and versatile approach, where hybrid numerical methods mixing both quantum and classical solvers can be applied to the different pieces of a fragmented material, Fig. 1. In DMET, low cost methods such as Hartree-Fock can be applied to non-active molecule fragments (*i.e.* not participating in a physical or chemical reaction studied), while active fragments can be handled using state-of-the-art quantum computing. As depicted in Fig. 1, CO_2 interaction with the Al-fumarate cluster is investigated to determine the adsorption energy associated with CO_2. An Al-fumarate molecule has one Al surrounded

Figure 1 A quantum computing methodology applied to CO_2 capture on Metal-Organic Frameworks. Al-fumarate molecule, a building block found in water stable MOF structures [23–26], has been chosen to investigate CO_2 adsorption in Al based MOFs as potential candidate for CO_2 capture [27, 28] (left). After fragmenting the fumarate (right), binding of the active Al site with the CO_2 molecule is determined by quantum computing, while fumarate fragments (gray bubbles) are treated with a classical computer quantum chemistry solver
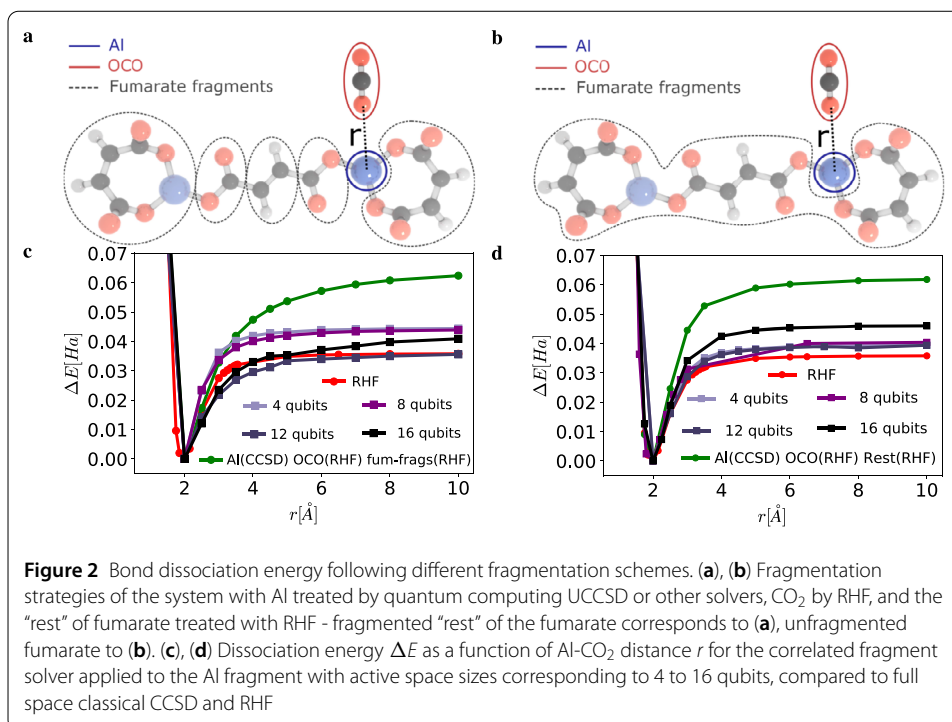
with oxygen atoms. In a realistic MIL-53(Al) two Al atoms would be relatively close by, even forming hydrogen bonds via their respective OH^- groups. However, since quantum computers are limited in computational space and since studies show that only one of the two neighboring Al atoms participates in CO_2 capture [42, 43] we chose the Al-fumarate molecule as a model system. Our choice of an Al-based MOF as a center of the study is also motivated with the fact that the electronic structure of Al-fumarate molecule could be relatively tame. In such a case low level solvers such as restricted Hartre-Fock provide a reasonable estimation to the ground state energy and could be used as a benchmark of the methodology itself.

The explicit calculation of the adsorption energy from first principles is intractable for large systems using brute force classical techniques due to the exponential scaling of the electronic structure problem. As indicated above, quantum computing techniques could overcome this problem, however devices which are sufficiently free from error, or which exhibit gate stabilities that allow for error-correcting schemes are still needed. In anticipation of this "fault-tolerant" regime [44], and to pave the way for future quantum simulations of solid-gas interactions, we study physical adsorption by NISQ-era algorithms. To do so, we use fragmentation strategies where the preferential adsorption site is solved by simulated quantum computation. In the latter, the adsorbing Al atom is treated with unitary coupled cluster truncated to singles and doubles excitations (UCCSD) [45], an ansatz for the electronic wavefunction that can be variationally optimised by quantum computing techniques such as the variational quantum eigensolver (VQE) [46].

VQE is a hybrid quantum-classical algorithm in which a quantum computer is used to store a quantum state, while measured values of its energy are fed to a classical computer which variationally optimises the energy. Technical details are provided in the Methods section. To limit the number of orbitals in the calculation (which reduces the number of qubits), some orbitals have been frozen out (electronic correlation not included), leaving an "active space" of orbitals contributing to the correlation, and in the context of the UCCSD ansatz we refer to this as AS-UCCSD. To compare the proposed approach to well established classical methods, fragments corresponding to low adsorption energy sites are also determined from classical solvers such as full space CCSD, mean-field restricted Hartree-Fock (RHF), and second-order Møller-Plesset perturbation theory (MP2), while fragments not directly involved in binding are limited to RHF (neglecting electronic correlation) or MP2 (a cheaper approximation to electronic correlation). The effects of different fragmentation scenarios with alternative solver mixing are presented and discussed in the Additional file 1.

In order to determine the Al-fumarate + CO_2 dissociation energy, we first approximate the minimum energy position of the CO_2 relative to the fumarate using classical methods (see Additional file 1). The total energy of the CO_2 + fumarate is then calculated by high accuracy quantum computing as a function of the distance (r) between the CO_2 molecule and the Al site of the fumarate for the two fragmentation schemes. In the first, Fig. 2a, Al is treated by AS-UCCSD, the whole CO_2 molecule by RHF, and the rest of the fumarate is fragmented and treated by RHF. In the second, Fig. 2b, the Al site (AS-UCCSD) and the CO_2 molecule (RHF) are embedded in a large mean-field environment, where the fumarate is treated as a single fragment (RHF). In both cases, quantum calculations are performed for different active spaces of the high level fragment, Fig. 2c,d, both showing a minimum energy at $\sim$2 Å. In Fig. 2c, the 4 qubit (1 HOMO 1 LUMO orbital) and 8 qubit

Figure 2 Bond dissociation energy following different fragmentation schemes. (**a**), (**b**) Fragmentation strategies of the system with Al treated by quantum computing UCCSD or other solvers, CO_2 by RHF, and the "rest" of fumarate treated with RHF - fragmented "rest" of the fumarate corresponds to (**a**), unfragmented fumarate to (**b**). (**c**), (**d**) Dissociation energy ΔE as a function of Al-CO_2 distance r for the correlated fragment solver applied to the Al fragment with active space sizes corresponding to 4 to 16 qubits, compared to full space classical CCSD and RHF

(2 HOMO 2 LUMO orbitals) cases show larger dissociation energy than RHF, while an active space of 12 qubits (3 HOMO 3 LUMO orbitals) tends to lower the bond dissociation energy back to the RHF value, and 16 qubits (4 HOMO 4 LUMO orbitals) increases the dissociation energy ($\Delta E(r = 10$ Å), which we refer to as ΔE from hereon in the text) to a value lying between the 8 qubit and RHF values. By comparison, the full-space CCSD solver for Al also exhibits a larger value than RHF, indicating that correlation contributes positively to ΔE, while also showing the qualitative consistency between quantum computational and high level classical approaches.

Dissociation energies corresponding to the second fragmentation (Fig. 2b), are shown in Fig. 2d. Here, we observe that the 16 qubit case for AS-UCCSD applied to the Al fragment moves the dissociation energy (relative to smaller active spaces) towards the full space CCSD curve. In Table 1, we show the difference between the classical CCSD and the quantum UCCSD as a function of active space for fragmentation Fig. 2b. Differences in ΔE, for comparable active spaces, are found <1 mHa. We also note key differences between the two fragmentations. While for both cases ΔE is significantly lower at 16 qubits compared to CCSD, fragmentation 2a shows a larger gap between AS-UCCSD and CCSD in ΔE). Also, fragmentation 2a exhibits smaller ΔE at 16 qubits than for 4 or 8 qubits, at variance to fragmentation 2b. This (combined with the small differences in correlation energy for larger active spaces shown in Fig. S4 and S5) suggest differences between these fragmentations in the treatment of correlation for UCCSD compared to CCSD, which may impact the long-range interactions between Al and CO_2. Comparing to results from the literature, we note that recent works have predicted binding energies of similar order of magnitudes from classical DFT calculations [43].

Note the sensitivity of DMET to fragmentation has been observed by our team for other molecules (not shown here), also revealing a strong qualitative dependence in ΔE depending on fragmentation schemes in those systems. It is also important to note that our results
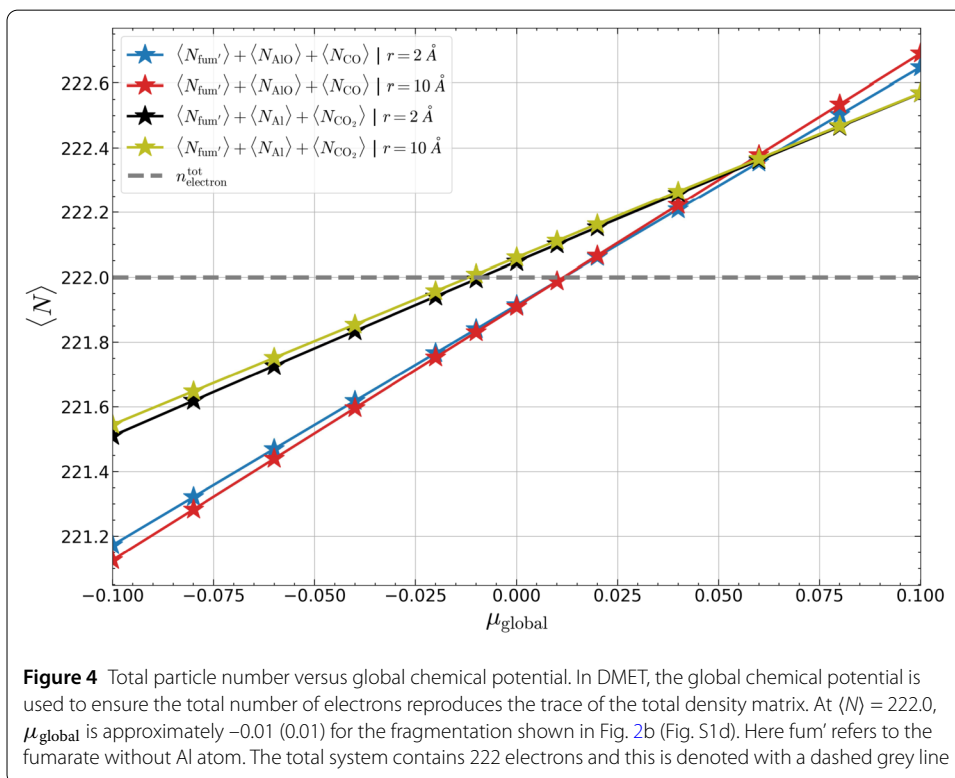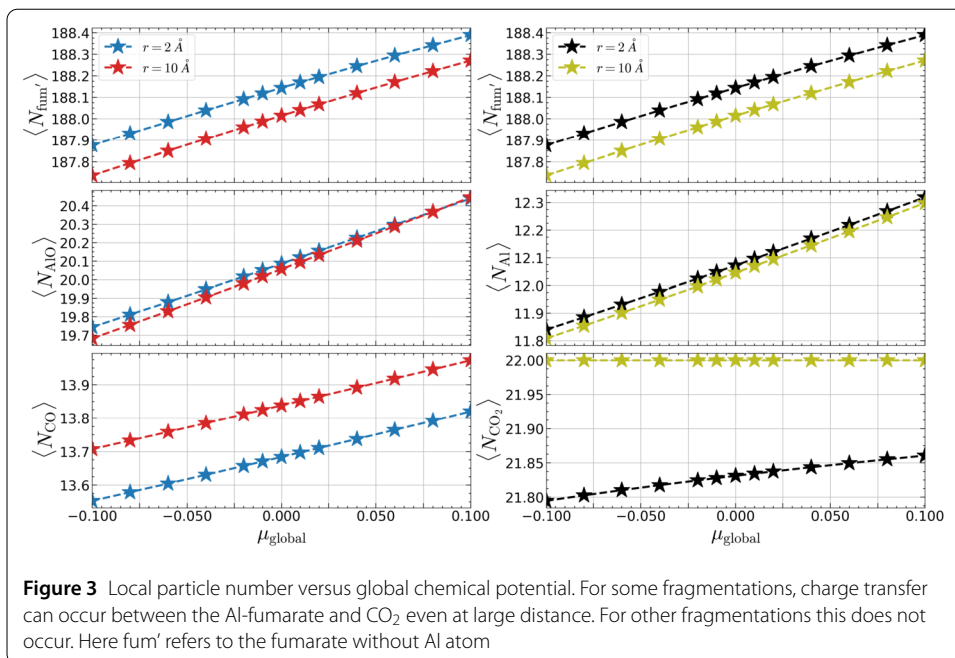
Table 1 Dissociation energy ($\Delta E(r = 10$ Å$)$) versus active space size for CCSD and UCCSD fragment solvers, using the fragmentation strategy depicted in Fig. 2b. For even numbers of active orbitals, equal numbers of occupied and unoccupied orbitals are used. For the case when 9 active orbitals are considered, 4 of them are HOMO and 5 of them LUMO

Nr. of active orbitals	0	2	4	6	8	9	10	12	14	16	18
$\Delta E_{CCSD}[10^{-3}Ha]$	35.8	39.6	40.3	39.6	46.5	51.6	51.2	62.1	57.7	60.4	61.8
$\Delta E_{UCCSD}[10^{-3}Ha]$	35.8	39.4	40.4	39.4	46.0	51.3	/	/	/	/	/
Difference	0	0.2	0.1	0.2	0.5	0.3	/	/	/	/	/

have strong implications for the notion of "democratic" mixing of local fragment properties (*e.g.* the fragment 1-RDM and 2-RDM-reduced density matrices-), reported to be sub-optimal when different solvers are applied to different fragments [41]. Contrary to these works, we demonstrate that when correlated fragment solvers (*i.e.* post-HF) are involved, physical dissociation curves are only found when different solvers are used for the fragment bonding to CO_2 and for the other fragments (Fig. S1 in Additional file 1). Therefore, we find that physically reasonable models of Al-fumarate + CO_2 dissociation can be obtained from DMET using democratic mixing of different solvers combined with the appropriate fragmentation. Overall, our results show that quantum computing methodologies can be used for studying these kinds of systems.

To go a step further, we investigate consequences of using the 1-shot version of DMET, where a global chemical potential μ_{global} is optimised such that the sum of fragment electron numbers matches the total number of electrons of the system, with no other parameters in the cost function of the DMET algorithm (details provided in Additional file 1). While such an approach leads to less variational flexibility, it benefits from higher efficiency and is commonly used in quantum computational applications [47–49]. Since the 1-shot DMET algorithm attempts to optimise a single global chemical potential, it stands to reason that unphysical dissociation in Fig. S1 may be related to the use of a single parameter to describe electron transfer between fragments. To investigate this hypothesis, we determined the local particle number of each fragment ($\langle N_x \rangle$ for fragment x) for a given μ_{global}, then sum over x to determine the total particle number ($\langle N \rangle$) of the system as a function of μ_{global}, Fig. 3 and 4. We then select the local particle number of each fragment for the chemical potential that conserves the total electron number ($\langle N \rangle = 222.0$), Table 2.

In the Fig. 4, we show that the total electron number is conserved for different chemical potentials depending on the fragmentation. When plots for the same fragmentation cross, the corresponding μ_{global} yields the same total electron number for different Al-O_{CO_2} distances, and these crossings occur at different points for different fragmentations, meaning that the relation between μ_{global} and r is not necessarily unique and depends on fragmentation. Moreover, for the CO_2 + Al fragmentation (Fig. 2) at $r = 10$ Å, the DMET chemical potential does not change $\langle N_{CO_2} \rangle$, corresponding to 22 electrons (see Fig. 3). As expected, the CO_2 is too far from the fumarate for charge transfer to occur. However, for the CO + (Al-O_{CO_2}) fragmentation (Fig. S1a,d), a charge transfer occurs even for large distances between the fumarate and CO_2. In other words, fragmentations shown in Fig. S1a,d do not prevent charge transfer through the whole system for any r, while that should be prevented for large Al-O_{CO_2} distances. This could explain why certain DMET fragmentations can fail.

Figure 3 Local particle number versus global chemical potential. For some fragmentations, charge transfer can occur between the Al-fumarate and CO_2 even at large distance. For other fragmentations this does not occur. Here fum' refers to the fumarate without Al atom

Figure 4 Total particle number versus global chemical potential. In DMET, the global chemical potential is used to ensure the total number of electrons reproduces the trace of the total density matrix. At $\langle N \rangle = 222.0$, μ_{global} is approximately −0.01 (0.01) for the fragmentation shown in Fig. 2b (Fig. S1d). Here fum' refers to the fumarate without Al atom. The total system contains 222 electrons and this is denoted with a dashed grey line

For the successful fragmentation strategies which exhibit physical dissociation curves, we show in Table 2 that decreasing r leads to a charge transfer from the CO_2 to the fumarate fragments not containing the adsorbing Al atom. As CO_2 moves from 10 Å to 2 Å, about 0.17 of a charge is transferred to the fumarate, $\sim$0.03 is localised on the Al atom, while the remaining charge is distributed to the rest of the fumarate (electron numbers are
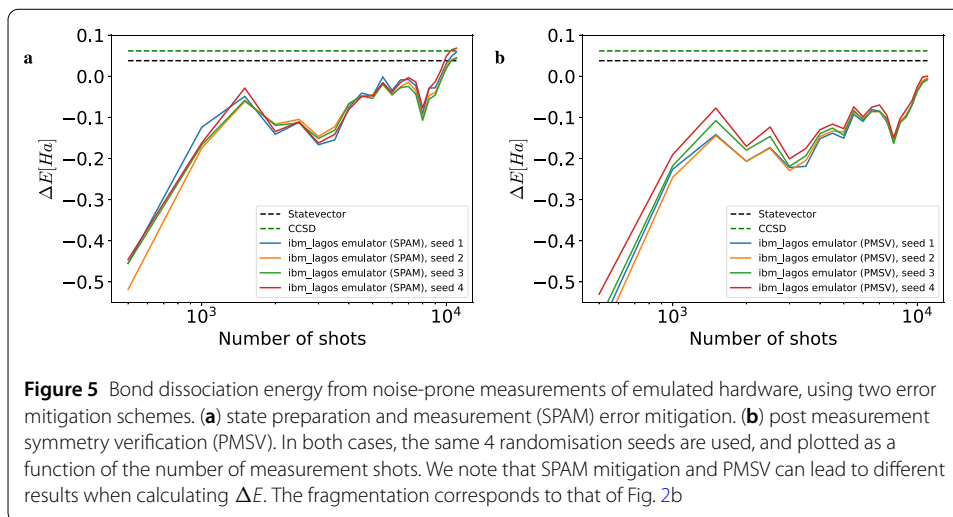
Table 2 Local electron number for $\mu_{\text{global}} \approx +0.01$ (fragmentation in Fig. S1d) and $\mu_{\text{global}} \approx -0.01$ (fragmentation in Fig. 2b). The rightmost column corresponds to a sum over fragments (x represents a fragment label), for which the total number should sum to 222 and the total charge transfer ($\langle \delta N \rangle$) should sum to 0, hence we note an error in electron number of approximately ± 0.01 due to lack to strict DMET cost optimisation

Fig. S1d fragmentation	$\langle N_{\text{CO}} \rangle$	$\langle N_{\text{AlO}} \rangle$	$\langle N_{\text{fum}'} \rangle$	$\sum_x$
$r = 2$ Å	13.6972	20.1216	188.1694	221.9881
$r = 10$ Å	13.8514	20.0954	188.0411	221.9878
$\langle \delta N \rangle$	−0.1542	0.0262	0.1283	0.0003

Fig. 2b fragmentation	$\langle N_{\text{CO}_2} \rangle$	$\langle N_{\text{Al}} \rangle$	$\langle N_{\text{fum}'} \rangle$	$\sum_x$
$r = 2$ Å	21.8278	12.0487	188.1180	221.9944
$r = 10$ Å	22.0000	12.0215	187.9876	222.0091
$\langle \delta N \rangle$	−0.172186	0.027151	0.13035	−0.0147

not strictly conserved to better than ± 0.01 in Table 2 since points on the $\langle N \rangle$ vs. μ_{global} line do not correspond to fully optimised DMET cost functions). As expected, this further confirms that the Al atom corresponds to the most favorable adsorption site. Thus, most of the electronic charge does not localise on the Al site in the adsorption process, but is found to be redistributed between the CO_2 and the rest of the fumarate. Thus, the successful DMET fragmentation strategy shows that a complex bond spanning many atoms is formed with Al acting as an intermediary conducting site.

Using the fragmentation shown in Fig. 2b, we also present dissociation barrier calculations resulting from emulated hardware measurements obtained with typical hardware noise on an IBMQ device. Error mitigation schemes are currently necessary to minimise the effects of hardware noise. However, the impact on dissociation energy of the choice of error mitigation scheme is not well known. We report the dissociation energy (ΔE) resulting from noisy measurements after applying one of two popular error mitigation schemes: mitigation of state preparation and measurement (SPAM) errors [50], and partition measurement symmetry verification (PMSV) [38, 51]. Due to the stochastic nature of the measurement process, we plot the measured ΔE versus number of measurement shots, where a larger number of shots corresponds to a better representation of the statistical distribution of measurement results. This is repeated using 4 randomisation seeds for both error mitigation schemes applied individually for the same calibration data, which provides a systematic comparison between the schemes. The results are plotted in Fig. 5.

It can be seen that for a sufficiently small number of measurement shots, the resulting ΔE can be negative (Fig. 5a,b). We also note that the measured total energies for both geometries (not shown for brevity) are below the ideal noise-free value. Thus a negative ΔE implies that device errors for this noise model have a slightly greater impact on the dissociated geometry. In addition, we observe that ΔE approaches the large-shot limit differently for SPAM error mitigation and for PMSV. Hence, to calculate energy barriers using error mitigated measurements on quantum hardware, it should be noted that different geometries (which correspond to different Hamiltonian parameters and different ansatz parameters) can lead to different behaviour of a given error mitigation scheme, and these differences can accumulate leading to additional errors in the calculated energy barrier.

Figure 5 Bond dissociation energy from noise-prone measurements of emulated hardware, using two error mitigation schemes. (**a**) state preparation and measurement (SPAM) error mitigation. (**b**) post measurement symmetry verification (PMSV). In both cases, the same 4 randomisation seeds are used, and plotted as a function of the number of measurement shots. We note that SPAM mitigation and PMSV can lead to different results when calculating ΔE. The fragmentation corresponds to that of Fig. 2b

3 Conclusions

The work presented here demonstrates the application of quantum computing methods as high-accuracy post-Hartree-Fock solvers in the treatment of carbon capture on Metal-Organic Frameworks (MOFs). Our findings suggest that quantum computing methodologies are successful in capturing many-body correlations in the MOF + CO_2 system, with physical dissociation curves. Furthermore, the versatility of the embedded quantum computational approach allows for estimates of the bond dissociation energy of the van der Waals molecule formed between CO_2 and the unit cell of the MOF. Finally, sampling the expectation value of the number operator on different fragments gives an insight into the complex bond which the CO_2 forms with the MOF. Although the CO_2 binds to the Al-site, a charge transfer between CO_2 and the rest of the fumarate molecule occurs, while the number of electrons on the Al-site remains largely unchanged. This indicates a non-trivial dependence of the CO_2 binding energy on MOFs - the energy depends both on the metal which is the active site but also on the atoms surrounding the metal. In addition, we provide results from emulated hardware experiments with two popular error mitigation schemes for the purpose of calculating chemical dissociation barriers, and we found significant differences between SPAM mitigation and PMSV, which relate to differences in how the mitigation schemes treat the different geometries. In summary, this work opens the pathway towards the use of quantum computing for complex materials design with strong molecular interactions in view of real world applications such as greenhouse gas capture.

4 Methods

In our calculations, we adopt a local cluster model of the full MOF supercell corresponding to the Al-fumarate molecule shown in Fig. 1, whose metal ion/oxide nodes correspond to low energy sites where the sorption usually occurs. Given that quantum computing calculations of complex systems are still relatively expensive, in terms of circuit depth and the number of qubits, calculations are made with the STO-3G minimal basis set. We note that while minimal basis sets are insufficient to capture all many-body interactions and hence prevent an accurate prediction of the binding energy, we use minimal basis sets in

order to qualitatively compare the performance of various post-HF methods and quantum computing methods as DMET solvers for this system.

In order to assess the minimum energy geometry of the combined Al-fumarate + CO_2 complex, geometry optimisation could be performed. However, long range dispersion interactions are not accurately captured at this level of theory. In particular, parameterised approximations to the dispersion interactions (such as DFT-D3 of Grimme et al. [52]) are not reliable when using a minimal basis set. This is especially true for a MOF interacting with CO_2 due to the complicated form of the guest-host exchange interaction, which DFT commonly fails to capture [20]. Hence, to assess the optimal geometry, we carry out simple tests of the Al-fumarate + CO_2 bonding configurations with classical computing methodologies, for which both the fumarate and the CO_2 are kept fixed at their isolated ground state geometries. Classical computing calculations with (coupled cluster singles doubles (CCSD) [53]) and without (Hartree-Fock (HF)) correlation of the combined Al-fumarate + CO_2 system were carried out for this purpose. These classical results serve as a guide for the combined quantum/classical simulations of the Al-fumarate + CO_2 system, in which the lowest energy bonding geometries (relative orientation, distance, incidence angle) can be assessed before tackling the problem with a quantum computational approach. From the results of the classical calculations, we select the bonding geometry of the Al-fumarate + CO_2 system to study using DMET with a quantum computational solver for the high accuracy fragment. Details and results of these classical calculations are reported in the Additional file 1.

All quantum calculations in this paper are performed using Quantinuum's computational chemistry platform [54]. This is a Python package for running quantum chemistry simulations on quantum computational hardware, built on top of the architecture agnostic quantum software compiler t|ket⟩^{TM} [55, 56]. Quantinuum's computational chemistry platform utilises the classical chemistry package PySCF [57] to generate classical data such as electronic integrals in the atomic orbital basis, in addition to classical methods such as HF, CCSD, and second-order Møller-Plesset perturbation theory (MP2) [58]. For HF calculations, we use the spin-restricted form (RHF) suitable for closed-shell systems. While all individual constituents of the Al-fumarate + CO_2 complex do not necessarily form a closed shell system, the DMET procedure itself generates a bath for each fragment, and each fragment + bath forms a closed shell system. The mapping of our quantum algorithms to quantum circuits is performed using t|ket⟩^{TM} [55] and Microsoft Azure is used as a platform for simulating idealised noise-free quantum hardware. For noisy simulations, we use the emulator of the *ibm_lagos* machine with a calibrated noise model, which is accessed via the IBMQ cloud service. This noise model includes qubit readout errors ranging from 5.1E−3 to 2.48E−2, single qubit Pauli-X errors ranging from 1.868E−4 to 3.025E−4, and CNOT errors ranging from 4.587E−3 to 1.037E−2. The full calibration data used for the simulation of this device is available from the authors on request. Two different error mitigation schemes are applied separately: state preparation and measurement (SPAM) [50] error mitigation, and partition measurement symmetry verification (PMSV) [38, 51]. For PMSV, we filter measurement shots for the $U(1)$ particle number symmetry. For more details on PMSV, we refer the reader to Yamamoto *et al.* [38]

Density Matrix Embedding Theory (DMET) [40, 41] is an embedding procedure based on the Schmidt decomposition of the wavefunction into fragments and their complementary parts, which self-consistently combines correlated solutions across the whole system.

A molecule is partitioned into a series of fragments, each one coupled to a bath that simulates the effect of the rest of the molecule. These reduced-size systems are then solved with different methods, with the most accurate method applied to the fragment representing the active site. More details about DMET can be found in Additional file 1.

There are many possible ways to fragment the Al-fumarate + CO_2 complex. We report four fragmentation strategies found to show drastically different results, and investigate these differences. By active site we refer to that part of the fumarate involved in CO_2 adsorption. For solving non-active sites of the fumarate we rely on classical computing methods such as HF, MP2 or coupled cluster theories (see Additional file 1 for more details). For solving the active site, we compare classical coupled cluster theory with a quantum Unitary Coupled Cluster ansatz with single and double excitations (UCCSD) implemented with a Variational Quantum Eigensolver (VQE) [46]. For the UCCSD fragment solver, orbital freezing was used to reduce the number of qubits required in the calculation and thus select an active space (AS-UCCSD). To investigate the effect of reducing the active space to feasible sizes, we plot the correlation energy as a function of active space size for all fragmentation strategies. The results, presented in the Additional file 1, show that a significant degree of correlation is captured by the active spaces used in this work.

VQE is a hybrid quantum-classical algorithm which relies on a quantum computer to estimate the expectation value of energy, while relying on a classical optimiser to suggest improvements of the ansatz [46]. In this work, we investigated the quantum UCC ansatz which has a complex circuit but is also (in principle) able to estimate the ground state energy of the system with higher precision. Thus, our strategy relies on UCC to obtain the ground state energy curve with the highest precision (see details in Additional file 1). For noise-prone simulations corresponding to the *ibm_lagos* emulator, we take the converged VQE parameters of the state vector (idealised) DMET calculation, and re-calculate the active fragment energy using the hardware emulator with a calibrated noise model.

A key quantity estimated is the CO_2-MOF bond stretching energy, $\Delta E(r) = E(r) - E(2\,\text{Å})$, which for $r \gg 2$ Å corresponds to the bond dissociation energy. This is justified as the CCSD numerical testing we performed showed that at 10 Å distance the energy gradient is less than 0.5 mHa/Å, hence the sum of the dissociated components is sufficiently well approximated by $E(10\,\text{Å})$. All energies are represented with respect to $E(2\,\text{Å})$, as classical calculations show that this is the bond distance between Al-fumarate and CO_2 which corresponds to the energy minimum (see Additional file 1 for details).

Supplementary information

Supplementary information accompanies this paper at https://doi.org/10.1140/epjqt/s40507-022-00155-w.

Additional file 1. Supplementary information (PDF 2.2 MB)

Availability of data and materials
The authors will make all data available upon reasonable requests.

Declarations

Ethics approval and consent to participate
Not applicable.

Consent for publication
Not applicable.

Competing interests
The authors declare no competing interests.

Author contributions
Author contributions G.G.D. and D.Z.M directly obtained the results presented in the study. G.G.D., D.Z.M., W.S., M.C., M.J.R., and D.M.R interpreted the data. E.S., P.L., P.C. M.J.R. and D.M.R. conceptualised the study. G.G.D, D.Z.M, Y.M., P.L., M.C. M.J.R and D.M.R. wrote and organised the paper. P.C, M.K., M.J.R. and D.M.R supervised parts of the conducted work. All coauthors participated in joint discussions. All authors read and approved the final manuscript.

Authors' information
Yann Magnin is consultant, on the behalf of TotalEnergies S.E.

Author details
[1]Cambridge Quantum Computing Ltd, 13-15 Hills Road, CB2 1NL, Cambridge, UK. [2]TotalEnergies, OneTech, One R&D, 8 Boulevard Thomas Gobert, 91120 Palaiseau, France. [3]TotalEnergies, OneTech, CO2 & Sustainability R&D, CSTJF - Avenue Larribau, 64018 Pau Cedex, France. [4]*Present address:* BMW Group, New Technologies and China, 80788 Munich, Germany.

Publisher's Note

Springer Nature remains neutral with regard to jurisdictional claims in published maps and institutional affiliations.

References

1. Odoh SO, Cramer CJ, Truhlar DG, Gagliardi L. Quantum-chemical characterization of the properties and reactivities of metal–organic frameworks. Chem Rev. 2015;115:6051–111. https://doi.org/10.1021/cr500551h.
2. Klimeš J, Michaelides A. Perspective: advances and challenges in treating van der Waals dispersion forces in density functional theory. J Chem Phys. 2012;137:120901. https://doi.org/10.1063/1.4754130.
3. Pachauri RK et al. Climate change 2014: synthesis report. Contribution of working groups I, II and III to the fifth assessment report of the intergovernmental panel on climate change (IPCC. 2014.
4. Tapia JFD, Lee J-Y, Ooi RE, Foo DC, Tan RR. A review of optimization and decision-making models for the planning of CO_2 capture, utilization and storage (CCUS) systems. Sustain Prod Consump. 2018;13:1–15. https://doi.org/10.1016/j.spc.2017.10.001.
5. Lecomte F, Broutin P, Lebas E. CO_2 capture: technologies to reduce greenhouse gas emissions. Editions Technip. 2010.
6. Gambhir A, Tavoni M. Direct air carbon capture and sequestration: how it works and how it could contribute to climate-change mitigation. One Earth. 2019;1:405–9. https://doi.org/10.1016/j.oneear.2019.11.006.
7. Lehtveer M, Emanuelsson A. BECCS and DACCS as negative emission providers in an intermittent electricity system: why levelized cost of carbon may be a misleading measure for policy decisions. Front Clim. 2021;3:647276. https://doi.org/10.3389/fclim.2021.647276.
8. Shen W, Fan W. Nitrogen-containing porous carbons: synthesis and application. J Mater Chem A. 2013;1:999–1013. https://doi.org/10.1039/C2TA00028H.
9. Liu Q, Pham T, Porosoff MD, Lobo RF. ZK-5: a CO_2-selective zeolite with high working capacity at ambient temperature and pressure. ChemSusChem. 2012;5:2237–42. https://doi.org/10.1002/cssc.201200339.
10. Wang H et al. Covalent triazine frameworks for carbon dioxide capture. J Mater Chem A. 2019;7:22848–70. https://doi.org/10.1039/C9TA06847C.
11. Gao Q et al. Synthesis of microporous nitrogen-rich covalent-organic framework and its application in CO_2 capture. Chin J Chem. 2015;33:90–4. https://doi.org/10.1002/cjoc.201400550.
12. Piscopo CG, Loebbecke S. Strategies to enhance carbon dioxide capture in metal-organic frameworks. ChemPlusChem. 2020;85:538–47. https://doi.org/10.1002/cplu.202000072.
13. Li H, Hill MR. Low-energy CO_2 release from metal-organic frameworks triggered by external stimuli. Acc Chem Res. 2017;50:778–86. https://doi.org/10.1021/acs.accounts.6b00591.
14. Collins SP, Daff TD, Piotrkowski SS, Woo TK. Materials design by evolutionary optimization of functional groups in metal-organic frameworks. Sci Adv. 2016;2:e1600954. https://doi.org/10.1126/sciadv.1600954.
15. Shekhah O, Liu J, Fischer R, Wöll C. MOF thin films: existing and future applications. Chem Soc Rev. 2011;40:1081–106. https://doi.org/10.1039/C0CS00147C.
16. Wilmer CE et al. Large–scale screening of hypothetical metal-organic frameworks. Nat Chem. 2012;4:83–9. https://doi.org/10.1038/nchem.1192.
17. Dureckova H, Krykunov M, Aghaji MZ, Woo TK. Robust machine learning models for predicting high CO_2 working capacity and CO_2/H2 selectivity of gas adsorption in metal organic frameworks for precombustion carbon capture. J Phys Chem C. 2019;123:4133–9. https://doi.org/10.1021/acs.jpcc.8b10644.
18. Bureekaew S et al. MOF-FF–a flexible first-principles derived force field for metal-organic frameworks. Phys Status Solidi (b). 2013;250:1128–41. https://doi.org/10.1002/pssb.201248460.
19. Boyd PG, Moosavi SM, Witman M, Smit B. Force-field prediction of materials properties in metal-organic frameworks. J Phys Chem Lett. 2017;8:357–63. https://doi.org/10.1021/acs.jpclett.6b02532.

20. Poloni R, Smit B, Neaton JB. CO_2 capture by metal-organic frameworks with van der Waals density functionals. J Phys Chem A. 2012;116:4957–64. https://doi.org/10.1021/jp302190v.
21. Vlaisavljevich B et al. Performance of van der Waals corrected functionals for guest adsorption in the M2 (dobdc) metal-organic frameworks. J Phys Chem A. 2017;121:4139–51. https://doi.org/10.1021/acs.jpca.7b00076.
22. Sladekova K et al. The effect of atomic point charges on adsorption isotherms of CO_2 and water in metal-organic frameworks. Adsorption. 2020;26:663–85. https://doi.org/10.1007/s10450-019-00187-2.
23. Alvarez E et al. The structure of the aluminum fumarate metal–organic framework A520. Angew Chem. 2015;127:3735–9. https://doi.org/10.1002/ange.201410459.
24. Bozbiyik B, Lannoeye J, De Vos DE, Baron GV, Denayer JF. Shape selective properties of the Al-fumarate metal–organic framework in the adsorption and separation of n-alkanes, iso-alkanes, cyclo-alkanes and aromatic hydrocarbons. Phys Chem Chem Phys. 2016;18:3294–301. https://doi.org/10.1039/C5CP06342F.
25. Tannert N, Jansen C, Niessing S, Janiak C. Robust synthesis routes and porosity of the Al-based metal–organic frameworks Al-fumarate, CAU-10-H and MIL-160. Dalton Trans. 2019;48:2967–76. https://doi.org/10.1039/C8DT04688C.
26. Ke F et al. Fumarate-based metal-organic frameworks as a new platform for highly selective removal of fluoride from brick tea. Sci Rep. 2018;8:1–11. https://doi.org/10.1038/s41598-018-19277-2.
27. Gaab M, Trukhan N, Maurer S, Gummaraju R, Müller U. The progression of Al-based metal-organic frameworks – from academic research to industrial production and applications. Microporous Mesoporous Mater. 2012;157:131–6. https://doi.org/10.1016/j.micromeso.2011.08.016.
28. Rouquerol J, Rouquerol F, Sing KS, Llewellyn P, Maurin G. Adsorption by powders and porous solids: principles, methodology and applications. San Diego: Academic Press; 2013.
29. Jajko G et al. Water adsorption in ideal and defective UiO-66 structures. Microporous Mesoporous Mater. 2021;330:111555. https://doi.org/10.1016/j.micromeso.2021.111555.
30. Magnin Y et al. A step in carbon capture from wet gases: understanding the effect of water on CO_2 adsorption and diffusion in UiO-66. J Phys Chem C. 2022;126:3211–20. https://doi.org/10.1021/acs.jpcc.1c09914.
31. Boyd PG et al. Data-driven design of metal–organic frameworks for wet flue gas CO_2 capture. Nature. 2019;576:253–6. https://doi.org/10.1038/s41586-019-1798-7.
32. Veis L, Pittner J. Quantum computing applied to calculations of molecular energies: CH_2 benchmark. J Chem Phys. 2010;133:194106. https://doi.org/10.1063/1.3503767.
33. Sugisaki K et al. Quantum chemistry on quantum computers: a method for preparation of multiconfigurational wave functions on quantum computers without performing post-Hartree-Fock calculations. ACS Cent Sci. 2019;5:167. https://doi.org/10.1021/acscentsci.8b00788.
34. Greene-Diniz G, Munoz Ramo D. Generalized unitary coupled cluster excitations for multireference molecular states optimized by the variational quantum eigensolver. Int J Quant Chem. 2021;121:e26352. https://doi.org/10.1002/qua.26352.
35. Liu J, Wan L, Li Z, Yang J. Simulating periodic systems on a quantum computer using molecular orbitals. J Chem Theory Comput. 2020;16:6904–14. https://doi.org/10.1021/acs.jctc.0c00881.
36. Yoshioka N, Sato T, Nakagawa YO, Ohnishi Y-Y, Mizukami W. Variational quantum simulation for periodic materials. Phys Rev Res. 2022;4:013052. https://doi.org/10.1103/PhysRevResearch.4.013052.
37. Manrique DZ, Khan IT, Yamamoto K, Wichitwechkarn V, Ramo DM. Momentum-space unitary coupled cluster and translational quantum subspace expansion for periodic systems on quantum computers. 2021. arXiv:2008.08694[quant-ph].
38. Yamamoto K, Manrique DZ, Khan I, Sawada H, Ramo DM. Quantum hardware calculations of periodic systems: hydrogen chain and iron crystals. 2022. arXiv:2109.08401[quant-ph].
39. Preskill J. Quantum computing in the NISQ era and beyond. Quantum. 2018;2:79. https://doi.org/10.22331/q-2018-08-06-79.
40. Knizia G, Chan GK-L. Density matrix embedding: a strong-coupling quantum embedding theory. J Chem Theory Comput. 2013;9:1428–32. https://doi.org/10.1021/ct301044e.
41. Wouters S, Jiménez-Hoyos CA, Sun Q, Chan GKL. A practical guide to density matrix embedding theory in quantum chemistry. J Chem Theory Comput. 2016;12:2706–19. https://doi.org/10.1021/acs.jctc.6b00316.
42. Serre C et al. An explanation for the very large breathing effect of a metal–organic framework during co2 adsorption. Adv Mater. 2007;19:2246–51.
43. Damas GB, Costa LT, Ahuja R, Araujo CM. Understanding carbon dioxide capture on metal–organic frameworks from first-principles theory: the case of MIL-53(X), with X = Fe3+, Al3+, and Cu2+. J Chem Phys. 2021;155:024701. https://doi.org/10.1063/5.0054874.
44. Egan L et al. Fault-tolerant control of an error-corrected qubit. Nature. 2021;598:281–6. https://doi.org/10.1038/s41586-021-03928-y.
45. Anand A et al. A quantum computing view on unitary coupled cluster theory. Chem Soc Rev. 2022;51:1659–84. https://doi.org/10.1039/D1CS00932J.
46. Peruzzo A et al. A variational eigenvalue solver on a photonic quantum processor. Nat Commun. 2014;5:4213. https://doi.org/10.1038/ncomms5213.
47. Li W, et al. Toward practical quantum embedding simulation of realistic chemical systems on near-term quantum computers. 2021. arXiv:2109.08062[quant-ph].
48. Kawashima Y, et al. Optimizing electronic structure simulations on a trapped-ion quantum computer using problem decomposition. 2021. arXiv:2102.07045[quant-ph].
49. Yamazaki T, Matsuura S, Narimani A, Saidmuradov A, Zaribafiyan A. Towards the practical application of near-term quantum computers in quantum chemistry simulations: a problem decomposition approach. 2018. arXiv:1806.01305[quant-ph].
50. Jackson C, van Enk SJ. Detecting correlated errors in state-preparation-and-measurement tomography. Phys Rev A. 2015;92:042312. https://doi.org/10.1103/PhysRevA.92.042312.
51. Kirsopp JJM et al. Quantum computational quantification of protein–ligand interactions. Int J Quant Chem. 2022;122(22):e26975. https://doi.org/10.1002/qua.26975.

52. Grimme S, Antony J, Ehrlich S, Krieg H. A consistent and accurate ab initio parametrization of density functional dispersion correction (DFT-D) for the 94 elements H-Pu. J Chem Phys. 2010;132:154104. https://doi.org/10.1063/1.3382344.
53. Bartlett RJ, Musiał M. Coupled-cluster theory in quantum chemistry. Rev Mod Phys. 2007;79:291–352. https://doi.org/10.1103/RevModPhys.79.291.
54. Quantinuum's computational chemistry platform. https://www.quantinuum.com/products.
55. Sivarajah S et al. t|ket〉: a retargetable compiler for NISQ devices. Quantum Sci Technol. 2020;6:014003. https://doi.org/10.1088/2058-9565/ab8e92.
56. https://cqcl.github.io/tket/pytket/api/index.html.
57. Sun Q et al. Recent developments in the pyscf program package. J Chem Phys. 2020;153:024109. https://doi.org/10.1063/5.0006074.
58. Szabo A, Ostlund N. Modern quantum chemistry: introduction to advanced electronic structure theory. New York: Dover; 1996.